Catalysis Today 266 (2016) 82–89

Contents lists available at ScienceDirect

Catalysis Today

journal homepage: www.elsevier.com/locate/cattod

Photocatalytic properties of boehmite–SnO_2 composites for the degradation of phenol

G. Mendoza-Damián[a,*], F. Tzompantzi[a,*], R. Pérez-Hernández[b], R. Gómez[a], A. Hernández-Gordillo[c,1]

[a] Depto. de Química, Área de Catálisis, Universidad Autónoma Metropolitana—Iztapalapa, Av. San Rafael Atlixco No. 186, México D.F. 09340, Mexico
[b] Instituto Nacional de Investigaciones Nucleares, Carretera México-Toluca S/N La Marquesa, Ocoyoacac, C.P. 52750 Edo. México, Mexico
[c] Instituto de Investigaciones en Materiales, Universidad Nacional Autónoma de México, Circuito Exterior SN, Ciudad Universitaria, C.P. 04510 México D.F., Coyoacán, Mexico

ARTICLE INFO

Article history:
Received 30 April 2015
Received in revised form 26 October 2015
Accepted 20 November 2015
Available online 11 January 2016

Keywords:
Boehmite–SnO_2 composites
Phenol
Photodegradation
Mineralization

ABSTRACT

Boehmite (AlOOH) and SnO_2 composites with different Sn^{4+} contents were obtained by the coprecipitation method, drying the materials at a desired temperature ranging from 100 to 250 °C. The photocatalytic properties of the composites were tested in the degradation and mineralization of phenol. The boehmite-SnO_2 composite with 10 mol% of Sn^{4+} featured an improved photocatalytic activity eliminating phenol under UV light irradiation, where the photodegradation rate was found to be 2.9 times more active than that of boehmite and bulk SnO_2. The photocatalytic activity of the composites was influenced by the optical-electronic properties displayed by the small SnO_2 particles. The drying temperature effect on the photocatalytic properties of the composites was also studied. The possible photocatalytic degradation mechanism was considered as a function of the interaction between boehmite and the small SnO_2 particles.

1. Introduction

Heterogeneous photocatalysis has recently attracted great attention for treating wastewater since the mineralization of persistent pollutants can be achieved under mild conditions using semiconductor materials. Nanocomposite oxide semiconductors are materials that have high surface areas and exhibit adequate hybrid properties that are synergistically derived from each component. These materials have generated great scientific and industrial expectations due to the diversity of chemical, physical and functional properties that are better than those displayed by the corresponding bulk materials [1,2].

Among the metal oxide semiconductors, SnO_2 has been recently studied due to its excellent chemical stability, electrical and optical properties and suitability to be used as optoelectronic devices, dye sensitized solar cells, gas sensors, electrode materials in Li/SnO_2 batteries and photocatalysts for the photodegradation of dyes and organic compounds [3,4]. SnO_2 is an n-type semiconductor with a wide band gap (Eg = 3.6 eV) and it has exhibited high photocatalytic activity under UV light irradiation, however, just like other metal oxide semiconductors such as TiO_2 and ZnO, SnO_2 has a low photocatalytic efficiency because of its wide band gap and high recombination rates of the photogenerated electron–hole pairs; in this sense, considerable efforts have been made to enhance its photoactivity [5,6].

On the other hand, it has been demonstrated that Al_2O_3 possesses photoactivity properties due to the fact that water molecules are physically adsorbed and also chemically bound on the Al_2O_3 surface. Some results reveal that phenol contaminants are absorbed on the Al_2O_3 surface and this may lead to the transfer of semiconductor photogenerated holes to the phenol molecule, resulting in enhanced photocatalysis rates [7]. Few studies have shown that by mixing Al_2O_3 with SnO_2, using a specific Al:Sn molar ratio and annealing at high temperatures from 400 to 800 °C, efficient materials such as hydroxylated Al_2O_3 [8] and Al_2O_3 doped with La [9] or Pr [10] anions can be synthesized in order to be used in either the photodegradation of phenol [11] or in the degradation of 4-nitrophenol [12]; these materials have shown to be more efficient than the pure SnO_2 nanoparticles because of the improved separation of charges occurring in the formed mixed oxide. The elimination of the phenol molecule via heterogeneous photocatalysis using nanocomposite oxides has opened a wide field in the environmental remedia-

* Corresponding authors.
E-mail addresses: zyanya_8@hotmail.com (G. Mendoza-Damián), fjtz@xanum.uam.mx (F. Tzompantzi).
[1] Catedrático Conacyt.

http://dx.doi.org/10.1016/j.cattod.2015.11.029
0920-5861/

tion research. Phenol compounds are considered as carcinogenic molecules and cannot be easily biodegraded due to their high chemical stability under natural environmental conditions [13].

Several partially-dehydrated-transition aluminas (aluminum hydroxides) with high specific surface areas and pore volumes have been widely used in the industry as adsorbents, ceramics, capacitors, substrates for integrated circuits and catalyst carriers. Among these materials, boehmite (AlOOH) has been the most important precursor or intermediary for the synthesis of alumina materials [14,15]. Boehmite exhibits a lamellar structure, where the Al^{3+} ions exist in distorted, edge-sharing octahedral arrays of oxide ions that form a double layer with layers being connected by zigzag chains of H-bonds. Due to the abundant surface hydroxyl groups (—OH), the interaction between boehmite and foreign molecules such as pollutant molecules via the formation of hydrogen bonds is expected, which facilitates the adsorption process and improves the degradation of the absorbed molecule [2,16].

In this work, boehmite-SnO_2 composites with different Sn^{4+} contents were prepared by the coprecipitation method and dried at a desired temperature within the 100–250 °C interval. The materials were characterized by different techniques such as XRD and UV–vis spectroscopy and tested in the degradation of phenol under UV light irradiation. The photocatalytic activity results of the composites with the optimum Sn^{4+} contents were discussed considering them as a function of the optical-electronic properties of SnO_2 and the presence of boehmite hydroxyl groups. The possible photodegradation mechanism is shown.

2. Experimental

2.1. Synthesis of boehmite-SnO_2 composites

Boehmite-SnO_2 composites with different Sn^{4+} molar ratios (5, 10, 15 and 20 mol%) were prepared by the coprecipitation method using $Al(NO_3)_3{\cdot}9H_2O$ (Merck) and $SnCl_4{\cdot}5H_2O$ (Merck). The metal precursors were dissolved in an aqueous solution and precipitated with urea (metal/urea molar ratio of 0.1) by hydrolyzation at 95 °C and pH of 8.5, leaving them aging for 36 h. The precipitated solid was recovered by filtration, washing it several times with H_2O and drying at 80 °C over all night. Afterwards, the materials were dried at a desired temperature ranging from 100 to 250 °C for 2 h. The samples were labeled as Bhte-SnX, where X represents the Sn^{4+} content (mol%). Separately, both boehmite and bulk unmodified SnO_2 were obtained as blank materials by following the same methodology described above and were labeled as Bhte and SnO_2, respectively. The bulk SnO_2 was dried at 150 °C.

2.2. Characterization of boehmite-SnO_2 composites

All the composites were characterized by X-ray diffraction using a BRUKER D2 PHASER diffractometer. Diffraction patterns were acquired between 5 and 70° 2θ with a 0.01 °s^{-1} step using a CuKa source (λ = 0.154 nm). The parameters of lattice, relative intensities and crystallite size were determined by using Bragg's law and Debye–Scherrer equation, considering that boehmite possessing a cubic structure. The absorption band of the samples was determined by reflectance diffuse spectroscopy UV–vis using a Varian Cary 100 spectrophotometer from 200 to 400 nm and the band-gap energy was calculated by applying the Kubelka–Munk method. TGA, TG-DTG thermograms of the samples were performed at up to 500 °C at a heating rate of 10 °C/min under static air atmosphere on a thermal analyzer apparatus PerkinElmer Diamond. FTIR absorption spectra of all the samples were recorded on a Shimadzu IR-440 FTIR spectrometer using an attenuated total reflection (ATR) accessory equipped with a ZnSe crystal. The measurements were performed at room temperature, at 815 Psi, and 250 scans at a resolution of 16 cm^{-1} in the range between 500 and 4000 cm^{-1} in the transmittance mode. The textural properties were analyzed on a QUANTACROME piece of equipment using N_2 as adsorbate at −196 °C. Prior to the analysis, the samples were desgased at 150 °C for 12 h.

2.3. Photocatalytic test in the degradation of phenol

The photocatalytic tests were performed in a home-made reactor using a solution of 40 ppm of phenol, 1 g/L of photocatalyst powder, magnetic stirring of 700 rpm, air flow of 1 mL/s and UV light irradiation (λ = 254 nm, 4400 $\mu W/cm^2$) delivered by a high pressure Hg lamp (Pen-Ray UV Lamp) placed into the solution covered with a quartz tube. Before the UV irradiation exposure, the suspension was left in the dark for 1 h at 700 rpm under air flow (1 mL/s) and then a suspension aliquot was taken in order to determine the adsorption phenomena. The phenol solution and intermediate products (catechol or hydroquinone, see SI, Fig. S0A) was analyzed by UV–vis absorbance spectroscopy using a Varian Cary 100 spectrophotometer, following the absorption bands of each component. Considering that the total absorption band represents the contribution of each component, depending on the absorption coefficient, we followed a methodology reported in the literature [17]. In our case, the concentration of each component was obtained from the absorbance data of the calibration curve of each component by solving the spectrum with the Excel SOLVER complement as shown in Supplementary information (see SI, Application of the Excel SOLVER tool in the solution of spectrum data). The Langmuir–Hinshelwood kinetic model is usually applicable to describe the kinetics of phenol degradation. Considering that phenol degradation is a pseudo first order reaction, the apparent rate constant (k_{app}) and phenol conversion products were obtained.

3. Results and discussion

3.1. Crystalline structure

The XRD patterns of boehmite (AlOOH) exhibit narrow reflection peaks that correspond to the (0 2 0), (0 2 1), (1 3 0) and (0 0 2 or 0 5 1) planes of the orthorhombic structure of the highly crystalline boehmite phase [18,19]. For all the boehmite-SnO_2 composites (Fig. 1A), in addition to the reflection peaks of the boehmite phase, broad reflection peaks at 26.95, 34.14 and 52.25° in 2θ, corresponding to the tetragonal structure of the nanocrystalline SnO_2 can be seen [20]. The intensity of these reflections increases as the Sn^{4+} content increases, while the reflections of the main boehmite plane (0 2 0) decrease in intensity. According to the relative plane intensities ($I_{Plane}/I_{(0\,2\,0)}$), the incorporation of Sn^{4+} into the boehmite structure modified the preferential growth in the (0 2 1, 1 3 0, and 0 0 2–0 5 1) planes, Fig. 1B. Thus, by incorporating 5 mol% of Sn^{4+} into the boehmite matrix, the growth of these planes was inhibited and by increasing the Sn^{4+} contents up to 10 mol%, only the (0 2 1) plane was grown. The average size of the boehmite crystallites in all the composites, calculated from the (0 2 0) plane using the Scherrer equation, was found within the 8–11 nm interval (Table 1), which is close to that of bulk boehmite, suggesting that the boehmite crystallite size was slightly affected by the SnO_2 presence. The average SnO_2 crystal size in all the composites could not be determined due to the overlapping of both the boehmite (0 2 1) plane and SnO_2 reflexion peaks. This result implies that SnO_2 is homogeneously dispersed into the boehmite matrix. The presence of both peaks suggests that the crystals are in contact with each other forming a composite type [21]. In addition, both crystallographic phases

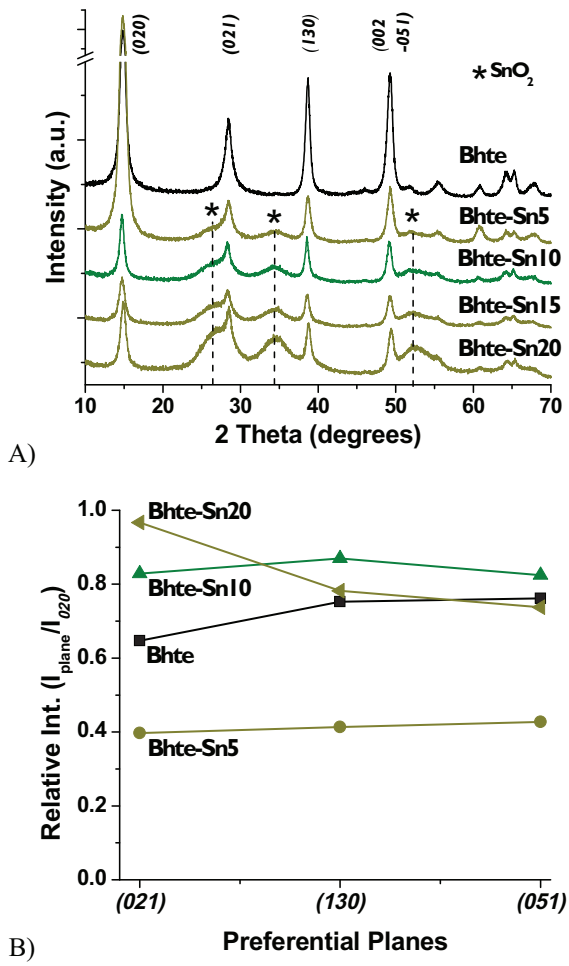

Fig. 1. (A) X-ray diffraction patterns of the Bhte and Bhte-SnO_2 composites and (B) comparison of relative intensity of (0 2 1), (1 3 0) and (0 5 1) planes.

Table 1
Data of specific surface area, crystallite size, band-gap energy and rate constant value.

Samples	Crystallite size AlOOH-SnO_2 (nm)	Band-gap (eV)		S_g (m^2/g) For 150 °C[a]
		For 100 °C	For 250 °C	
Bhte	10.2, –	5.50	5.51	61
Bhte-Sn5	08.6, –	4.59	4.54	111
Bhte-Sn10	11.5, –	4.54	4.46	127
Bhte-Sn15	09.8, –	4.50	4.42	156
Bhte-Sn20	10.5, –	4.46	4.35	176
SnO_2	–, 2.4	4.00	3.80	213

S_g = Specific surface area, a = selected temperature due to the high photoactivity of Bhte-Sn10 composite.

remain in the samples dried at 250 °C (see SI, Fig. S1) since the reflection peaks do not evolve.

3.2. TG and TA analysis

The TG and TA analysis results for boehmite exhibit weight loss at 250 °C (7 wt.%), but higher weight loss is observed from 380 to 450 °C. The first weight loss is associated with the elimination of water adsorbed on the boehmite surface and the second one is related to dehydroxylation to form Al_2O_3 [19]. The boehmite-SnO_2 composite with 10 mol% of Sn^{4+} (Fig. 2) shows weight loss at 250 °C (10 wt.%) that is similar to that of boehmite, which is related to

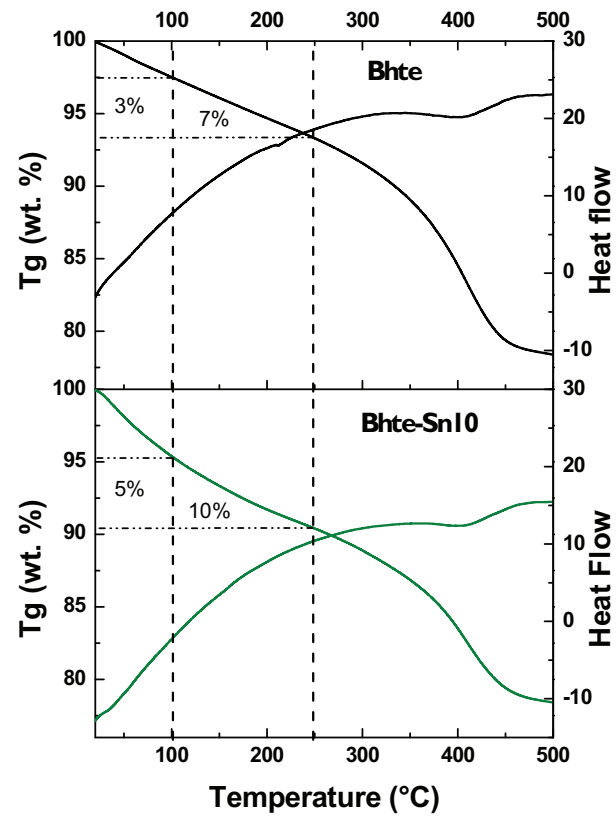

Fig. 2. TG and TA analysis of the Bhte and Bhte-Sn10 composite dried at 100 °C.

the removal of physisorbed water [21]. This result suggests that structural water and the high amount of hydroxyl groups on the composite surface are not affected by the drying temperature at 250 °C, which is in good agreement with the boehmite phase in the composites dried at 250 °C (see SI, Fig. S1).

3.3. Surface hydroxyl groups (FTIR analysis)

The IR spectra of boehmite samples dried at different temperatures from 100 to 250 °C (Fig. 3) exhibit characteristic bands of boehmite hydroxyl groups. The two peaks at 3286 and 3086 cm^{-1} correspond to —OH stretching frequencies of the hydroxyl group within the structure of the well crystallized boehmite phase [22,23]. However, as the drying temperature increases, the intensity of the peaks at 1145 and 1063 cm^{-1}, corresponding to the bending vibration of Al—OH in-plane (δOH), is slightly decreased [24,25]. Finally, the presence of the peak at 733 cm^{-1}, which corresponds to the bending vibration of Al–OH out-of-plane (γOH), is also increased. This —OH bending vibration indicates that these groups are on the boehmite surface.

For the Bhte-Sn10 composite dried at 100 °C, the IR spectrum shows the peaks (at 3286 and 3086 cm^{-1}) of —OH stretching frequencies of crystallized boehmite; in addition, it also exhibits peaks at 1063 and at 733 cm^{-1}. Typically, the bending vibration of coordinated —OH from the Sn—OH bond (see SI, Fig. S2) appears at 1620–1640 cm^{-1} [4], which is absent in all the composites due to the low Sn^{4+} contents. The peaks at 1145, 1063 and 733 cm^{-1}, related to the boehmite hydroxyl surface, are absent in the bulk SnO_2 (Fig. S2). By comparing bulk SnO_2 with the boehmite-SnO_2 composite, the boehmite absorption peaks were unmodified, indicating that the presence of the SnO_2 particles does not affect the hydroxyl surface (Al—OH in-plane and out-of-plane) due to the

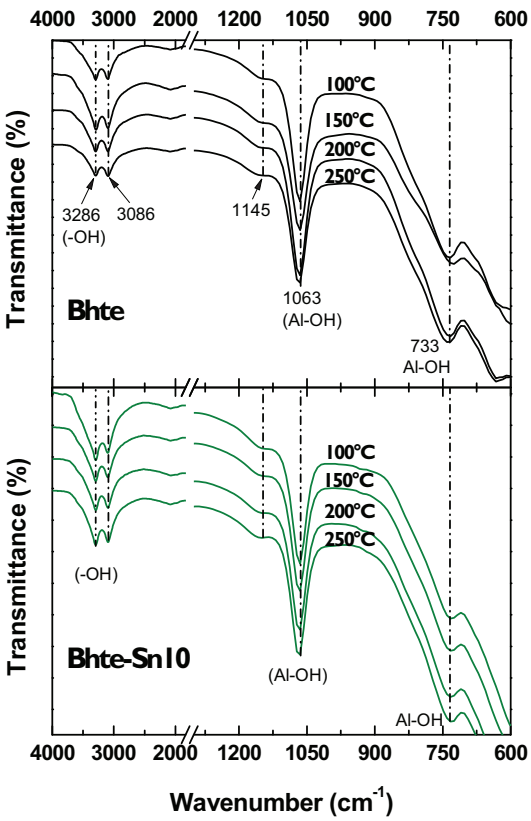

Fig. 3. FTIR spectra of the Bhte and Bhte-Sn10 composite dried at different temperature from 100 to 250 °C.

Table 2
Data of atomic composition and molar ratio of Sn^{4+} ions on the selected samples.

Samples	Atomic composition			Molar ratio (Sn%)
	O	Al	Sn	
Bhte	76.82	23.18	0.00	00.0
Bhte-Sn10	74.59	23.24	2.17	08.5
Bhte-Sn20	80.69	15.90	3.38	17.5

high dispersion in all the boehmite matrix. A similar behavior was observed for the other composite materials (see SI, Fig. S3).

3.4. Morphological and textural properties

The boehmite SEM image together with the EDX spectra (Fig. 4A) reveal that the particles have large size platelet or sheet morhoplogies (microns) and the atomic ratio (Al/O = 0.30) is slightly lower than the theoretical value (Al/O = 0.31), indicating oxygen excess in the boehmite matrix. The SEM elemental mappings of large particles in the Bhte-Sn10 and Bhte-Sn20 samples together with EDX spectra (Fig. 4B and C) reveal that the Sn distribution is overlapped with O and Al, indicating that Sn coexists and is well dispersed in every individual particle; this finding could be attributed to the synthesis method used in this work. In addition, the EDX analysis for the Bhte-Sn10 and Bhte-Sn20 samples (Table 2) shows that the molar ratio of the Sn contents is slightly lower than that of the theoretical loading, indicating that the used Sn content is almost fully incorporated into the boehmite matrix.

In order to have more specific information about the morphology, composition and Sn distribution of the prepared samples, TEM measurements were performed for the selected sample. The TEM analysis of the AlOOH powder (Fig. 5A) shows large aggregates with irregular form, which was retained after the Sn addition and thermal treatment, however, according to the EDX analysis, additional numerous black spots attributable to Sn nanoparticles were detected. It is evident that the distribution of SnO_2 particles in the boehmite matrix is homogeneous and the particle sizes are approximately 5 nm in diameter (Fig. 5B). In addition, the specific surface areas for boehmite and bulk SnO_2 are 61 and 213 m^2/g, respectively, and for the composites are between 111 and 176 m^2/g, respectively, Table 1. This increment is related to the increasing Sn contents.

3.5. Optical properties

The optical absorption studies for boehmite (Fig. 6) show a small absorption band from 190 to 230 nm, centered mainly at 206 nm, which is characteristic of aluminum hydroxide and aluminum oxide. Considering its dielectric nature, this electronic transitions are originated by the presence of surface defects (anion vacancies) called F* centers, which consist of an oxygen vacancy with a single trapped electron [4,26]. When boehmite contains 5 mol% of Sn^{4+}, the absorption band centered at 217 and 251 nm appears and for the composites with high Sn^{4+} contents (>10 mol%), this broad band at 217–300 nm (centered mainly at 251 nm) increases, which is associated with the electronic transition of SnO_2 incorporated into the boehmite matrix.

The absorption bands built up at 228 and 266 nm for the bulk SnO_2 are assigned to charge transfer transitions of $O^{2-} \rightarrow Sn^{4+}$, where the Sn ions are in tetrahedral (Th) and octahedral (Oh) coordinations, respectively [27]. This result suggests that the blue-shifted absorption band (251 nm) for the composites is due to the presence of the quantum confinement effect caused by the small SnO_2 particle size [28,29]. The band-gap energy for boehmite is 5.5 eV, but when the composite is formed, the band-gap energy decreases from 4.59 to 4.46 eV as Sn^{4+} increases (Table 1). This band-gap result can be due to the small crystallite size of SnO_2 formed into the boehmite matrix. The band-gap energy for bulk SnO_2 is close to 4.0 eV. Once the composites were dried at 250 °C, the band-gap energy slightly decreased due to the sinterization or segregation of SnO_2 particles (see Table 1).

3.6. Photodegradation of phenol

The UV–vis absorbance spectra of phenol photodegradation using the boehmite photocatalyst (Fig. 7A) show that the absorption band at 268 nm, characteristic of phenol compounds, slightly decreased, whereas a new absorption band at 287 nm was increased as the time passed. This last absorption band is related to the presence of intermediaries (Hydroquinone), however, phenol was not completely degradated. Conversely, when the Bhte-Sn10 composite was used, both phenol and hydroquinone absorption bands were completely decreased during the UV-irradiation (120 min) of the solution (Fig. 7B). A residual band from 190 to 230 nm, corresponding to residual organic acid, is observed for all the composites. The absorbance spectra of phenol photodegradation using the other composites are presented in the SI, Fig. S4.

The kinetic behavior for both boehmite and the Bhte-Sn10 composite follow a pseudo first order reaction (Fig. 8A). Thus, the apparent rate constant value of boehmite (3.0×10^{-3} min^{-1}) in the photodegradation of phenol was improved by 2.6 times when it is combined with 10 mol% of Sn^{4+} (Fig. 8B), achieving an apparent rate constant value of 8.6×10^{-3} min^{-1}, which is even 3.3 times more active than TiO_2-P25 (2.4×10^{-3} min^{-1}) used as a reference. The apparent rate constant value for the composites with 15 and 20 mol% of Sn^{4+} was poorly improved by 2.9 and 3.3 times of activity, respectively.

In addition, boehmite and the selected composites (Bhte-Sn10 and Bhte-Sn15) dried at 100, 150, 200 and 250 °C showed similar apparent rate constant values within this temperature interval

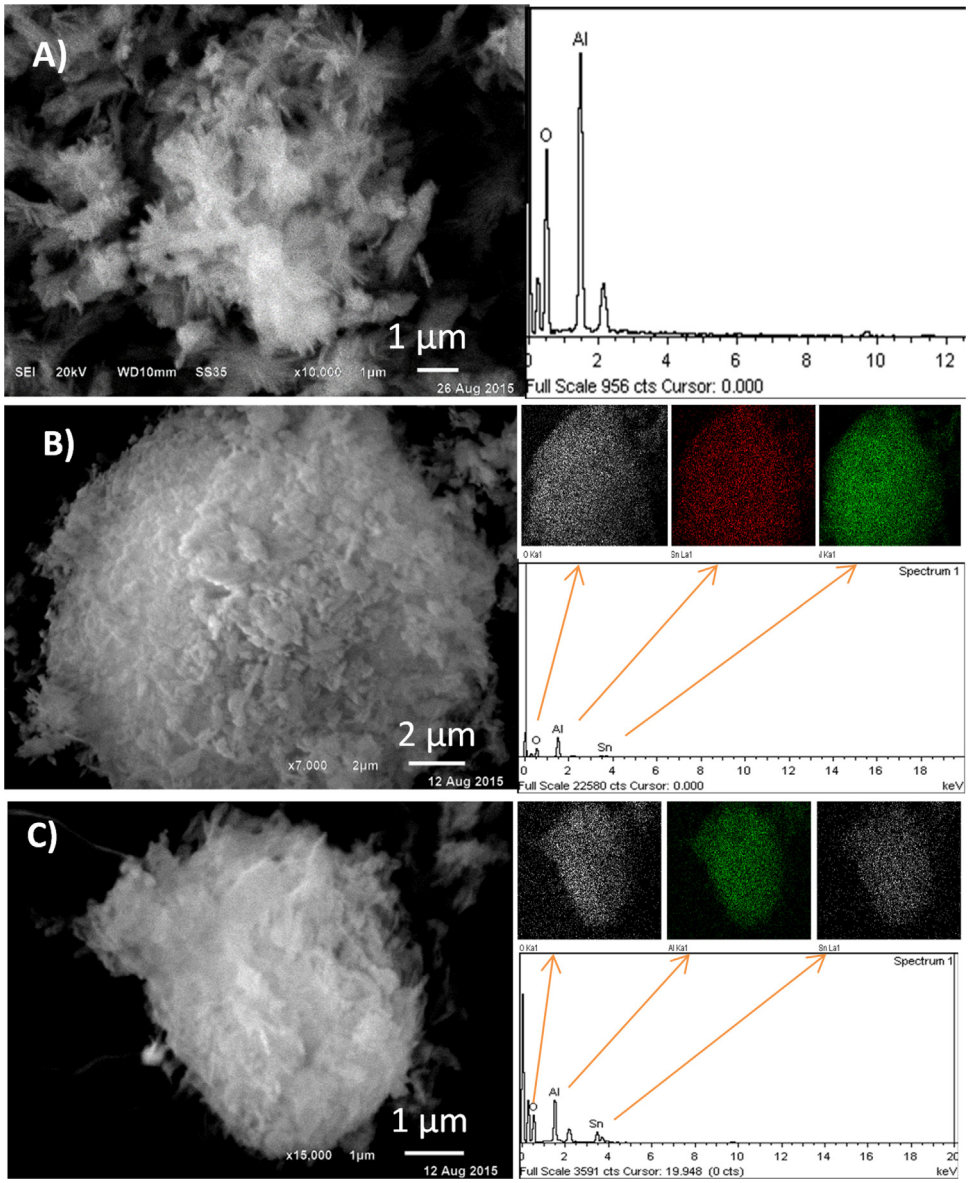

Fig. 4. SEM image and EDS elemental chemical mapping of the (A) AlOOH (B) Bhte-Sn10 and (C) Bhte-Sn20 samples, respectively on a single large grain.

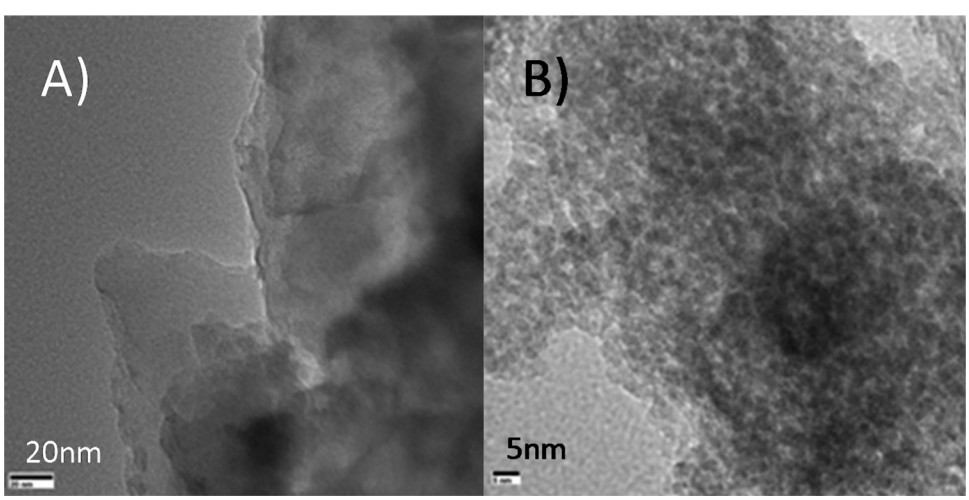

Fig. 5. TEM image of the (A) AlOOH and (B) Bhte-Sn10 composite dried at 100 °C.

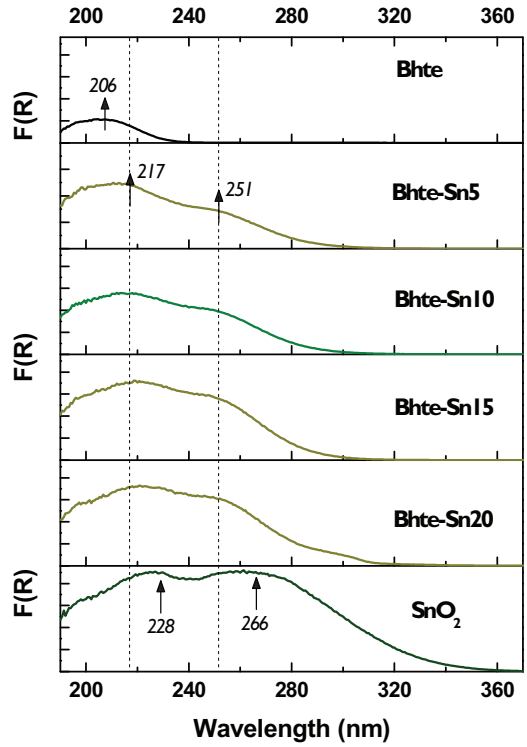

Fig. 6. Reflectance diffuse UV–vis spectra of the Bhte, SnO_2 and Bhte-SnO_2 composite dried at 100 °C and 250 °C.

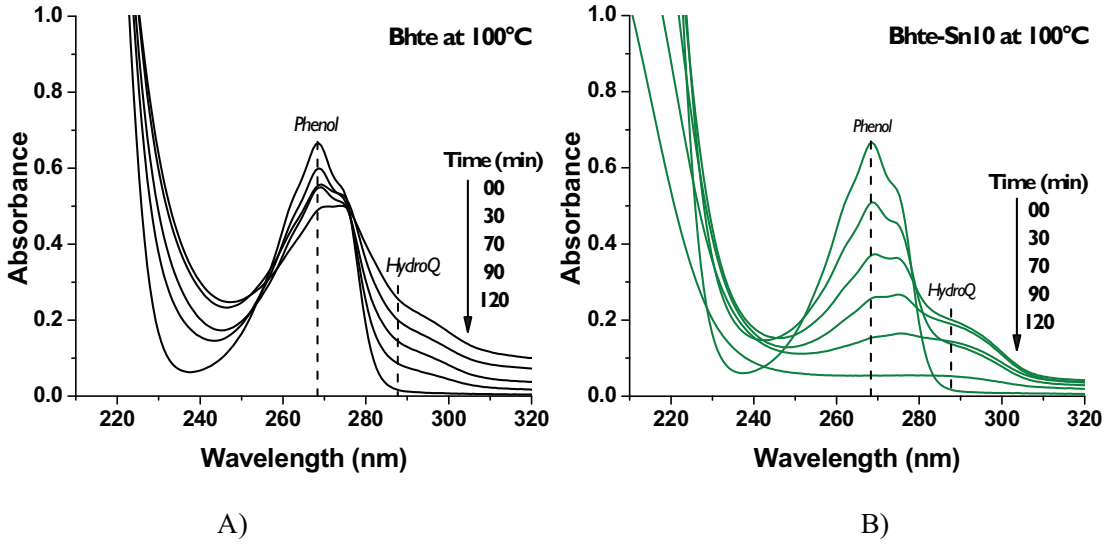

Fig. 7. Absorbance spectra of phenol degradation using: (A) Bhte and (B) Bhte-Sn10 photocatalysts dried at 100 °C.

(Fig. 9A), however, the highest photocatalytic activity of the Bhte-Sn10 composite was maintained. The low photocatalytic activity for the boehmite dried at this temperature interval was unaltered. The phenol mineralization percents obtained with TiO_2-P25 was 29% (not shown) and 22% by using the Bhte-Sn10 composite dried at 100 °C (Fig. 9B), however, when it was dried at 150 °C, the phenol mineralization percent was increased to 48%, suggesting that the phenol compounds were oxidized up to CO_2 formation. The phenol mineralization percents obtained using the Bhte-Sn10 composite dried at 200 and 250 °C were 30 and 25%, respectively. This low phenol mineralization suggests a high content of organic acids in the final irradiated solution.

3.7. Photodegradation mechanism

Considering that boehmite is a dielectric material, the presence of surface defects (anion vacancies), called F^* centers, can photogenerate electron–hole charges, exhibiting photocatalytic properties because of the excited state to which the electron is raised upon the absorption of a photon, which is very close to the crystal conduction band [30]; so, either the electron or the hole can react with O_2 or OH^- to generate •OH radicals, which are powerful oxidizing agents to carry out the degradation of phenol compounds, however, this process is improved when boehmite is combined with small SnO_2 particles because these particles extend

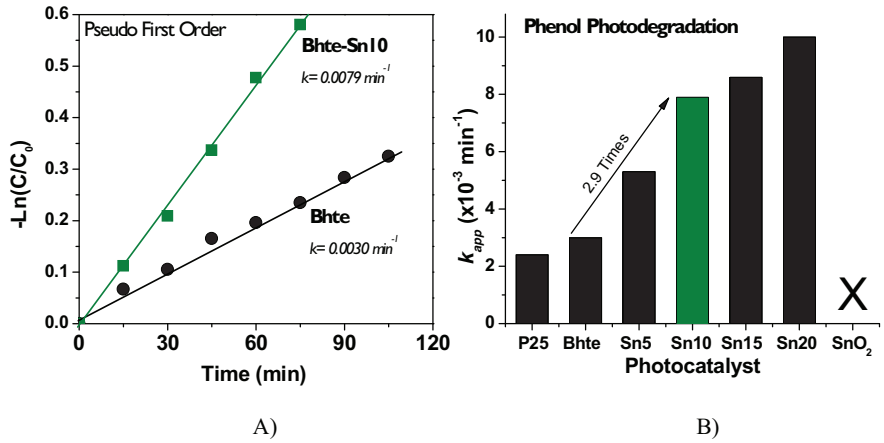

Fig. 8. (A) Kinetic behavior and (B) pseudo first order rate constant value of the all photocatalysts dried at 100 °C, evaluated in the photodegradation of phenol. P25 is used as reference photocatalyst.

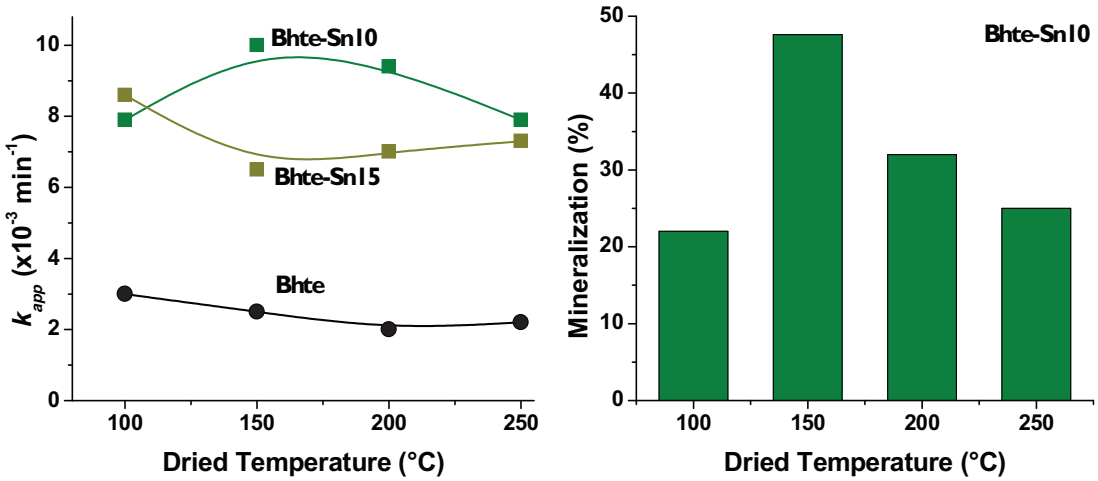

Fig. 9. (A) Pseudo first order rate constant value for the selected photocatalysts, (B) mineralization percent of the selected Bhte-Sn10 composite, evaluated in the photodegradation of phenol as function of dried temperature.

the UV absorption and contribute to the separation of photogenerated electron–hole charges.

4. Conclusions

The combination of boehmite with small SnO_2 particles modified the optical and electronic properties of composites and, as consequence, their photocatalytic properties were improved. The presence of SnO_2 into the boehmite matrix hindered the crystallization of boehmite, decreasing its crystallinity. The boehmite UV absorption was extended by the SnO_2 presence and the photocatalytic efficiency in the photodegradation of phenol was improved 2.6 times in comparison with boehmite due to the separation of the electron–hole charge. Little effect was observed by the drying temperature, where the most photoactive catalyst was the composite dried at 150 °C.

Acknowledgments

The authors thank CONACYT for the financial support provided for the development of the present research work (project 154994, Elimination of contaminant molecules by using a lamellar oxide), and for the support granted to Guadalupe Mendoza Damián (scholarship 252087). The authors would like to acknowledge PhD. Gilberto Mondragón Galicia for the TEM analyses.

Appendix A. Supplementary data

Supplementary data associated with this article can be found, in the online version, at http://dx.doi.org/10.1016/j.cattod.2015.11.029.

References

[1] S.-W. Lee, F. Paraguay-Delgado, R.D. Arizabalo, R. Gómez, V. Rodriguez-González, Mater. Lett. 107 (2013) 10–13.
[2] F. Chang, M. Zhang, G. Wang, W. Shi, X. Hu, Water Air Soil Pollut. 223 (2012) 2073–2081.
[3] M. Parthibavarman, K. Vallalperuman, S. Sathishkumar, M. Durairaj, K. Thavamani, J. Mater. Sci. Mater. Electron. 25 (2014) 730–735.
[4] A.E. Shalan, I. Osama, M.M. Rashad, I.A. Ibrahim, J. Mater. Sci. Mater. Electron. 25 (2014) 303–310.
[5] S.A. Ansari, M.M. Khan, M.O. Ansari, J. Lee, M.H. Cho, New J. Chem. 38 (2014) 2462–2469.
[6] Z. He, J. Zhou, Modern Res. Catal. 2 (2013) 13–18.
[7] C. Karunakaran, R. Dhanalakshmi, P. Gomathisankar, Res. Chem. Intermed. 36 (2010) 361–371.
[8] F. Tzompantzi, Y. Piña, A. Mantilla, O. Aguilar-Martínez, F. Galindo-Hernández, X. Bokhimi, A. Barrera, Catal. Today 49 (2014) 220–222.

[9] F. Tzompantzi, Y. Carrera, G. Morales-Mendoza, G. Valverde-Aguilar, A. Mantilla, Catal. Today 212 (2013) 164–168.
[10] A. Barrera, F. Tzompantzi, J.M. Padilla, J.E. Casillas, G. Jácome-Acatitla, M.E. Cano, R. Gómez, Appl. Catal. B: Environ. 144 (2014) 362–368.
[11] C.-Y. Kuo, React. Kinet. Catal. Lett. 92 (2007) 337–343.
[12] L. Xi, D. Qian, X. Huang, H.-E. Wang, J. Alloys Comp. 462 (2008) 42–46.
[13] G. Busca, S. Berardinelli, C. Resini, L. Arrighi, J. Hazard. Mater. 160 (2008) 265–288.
[14] H. Liang, L. Liu, H. Yang, J. Wei, Z. Yang, Y. Yang, Cryst. Eng. Commun. 13 (2011) 2445–2450.
[15] F. Meng, G. Rong, X. Zhang, W. Huang, Mater. Lett. 129 (2014) 114–117.
[16] X. Yu, J. Yu, B. Cheng, M. Jaroniec, J. Phys. Chem. C 113 (2009) 17527–17535.
[17] R. Su, R. Tiruvalam, Q. He, N. Dimitratos, L. Kesavan, C. Hammond, J.A. Lopez-Sanchez, R. Bechstein, C.J. Kiely, G.J. Hutchings, F. Besenbacher, ACS Nano 6 (7) (2012) 6284–6292.
[18] Z. Zhang, T.J. Pinnavaia, Langmuir 26 (2010) 10063–10067.
[19] P. Alphonse, M. Courty, Thermochim. Acta 425 (2005) 75–89.
[20] H. Benhebal, M. Chaib, A. Léonard, S.D. Lambert, M. Crine, J. Mol. Struct. 1004 (2011) 222–226.
[21] Z.K. Heiba, M.A. Ahmed, S.I. Ahmed, J. Alloys Compd. 507 (2010) 253–256.
[22] H.D. Ruan, R.L. Frost, J.T. Kloprogge, J. Raman Spectrosc. 32 (2001) 745–750.
[23] S. Musić, Đ. Dragčević, S. Popović, Mater. Lett. 40 (1999) 269–274.
[24] D.G. Lewis, V.C. Farmer, Clay Miner. 21 (1986) 93–100.
[25] R. Petrovic, S. Milonjic, V. Jokanovic, Lj. Kostic-Gvozdenovic, I. Petrovic-Prelevic, Dj. Janackovic, Powder Technol. 133 (2003) 185–189.
[26] Z.Q. Yua, C.X. Wanga, X.T. Gu, C. Li, J. Lumin. 106 (2004) 153–157.
[27] E.M. Seftel, E. Popovici, M. Mertens, P. Cool, E.F. Vansant, J. Optoelectron. Adv. Mater. 10 (2008) 3477–3481.
[28] L. Yao, Y.C. Zhang, J. Li, Y. Chen, Sep. Purif. Technol. 122 (2014) 1–5.
[29] P. Baraneedharan, C. Siva, K. Nehru, M. Sivakumar, J. Mater. Sci. Mater. Electron 25 (2014) 255–261.
[30] A.V. Emeline, G.V. Kataeva, V.K. Ryabchuk, N. Serpone, J. Phys. Chem. B 103 (1999) 9190–9199.